Journal of Catalysis 260 (2008) 276–287

Contents lists available at ScienceDirect

Journal of Catalysis

www.elsevier.com/locate/jcat

A DFT study of the origin of the HDS/HydO selectivity on Co(Ni)MoS active phases

E. Krebs [a,b], B. Silvi [b], A. Daudin [c], P. Raybaud [a,c,*]

[a] IFP, Direction Chimie et Physico-Chimie Appliquées, 1-4, Avenue de Bois-Préau, 92852 Rueil-Malmaison Cedex, France
[b] Université Pierre et Marie Curie, Laboratoire de Chimie Théorique, UMR 7616, 3, Rue Galilée, 94200 Ivry Sur Seine, France
[c] IFP, Direction Catalyse et Séparation, Rond-Point de l'Échangeur de Solaize, BP 3, 69360 Solaize, France

ARTICLE INFO

Article history:
Received 25 July 2008
Revised 29 September 2008
Accepted 29 September 2008
Available online 23 October 2008

Keywords:
Hydrodesulfurization
Hydrogenation of olefins
CoMoS
NiMoS catalysts
First principles
DFT
Selectivity
Volcano curves

ABSTRACT

Using first-principles calculations, we investigate the selective adsorption of 2-methylthiophene and 2,3-dimethylbut-1-ene on the Co(Ni)MoS active edge sites. These two model molecules being relevant for the selective HDS/HydO reaction of FCC gasoline, it is shown that their relative adsorption energies at the edges must be regarded as a key chemical descriptor governing the resulting HDS/HydO selectivity. The experimentally observed higher selectivity of CoMoS is explained on the basis of the reactants adsorption selectivity and the evaluation of the active edge energies with the adsorbed reactants. The effects of the promoter content, the morphology (S-edge/M-edge) and the H_2S/H_2 partial pressure on the selectivity descriptor are investigated in details. A consistent comparison with recent kinetic modeling of the HDS/HydO selectivity is provided on the basis of volcano-curves relationships.

1. Introduction

Among the processes used to refine petroleum cuts, hydrotreatment processes are of major importance to reach international fuel standards. In particular, the hydrodesulfurization (HDS) is a key process to reduce sulfur contents in diesel and gasoline below 10 ppm. These environmental constraints represent a driven force for the continuous improvement of the γ alumina Co(Ni)MoS supported catalysts widely used in the refining industry [1,2]. The HDS of gasoline produced from the fluid catalytic cracking (FCC) unit requires a selective sulfur removal from thiophene derivatives while avoiding the hydrogenation of olefins (HydO) present in FCC gasoline. This represents a technical challenge to prevent the loss of octane number of gasoline. From a scientific point of view, it is still an open question why the CoMoS active phase exhibits an improved HDS/HydO selectivity with respect to NiMoS, often recognized as being "more hydrogenating." The HDS/HydO selectivity has been the subject of recent experimental works on model molecules for FCC gasoline or real feed [3–8]. Furthermore, the kinetic investigation by Daudin et al. [9] has revealed a volcano-curve relationship between the experimental HDS/HydO selectivity of model molecules on transition metal sulfides (TMS) and the calculated values of the sulfur–metal bond energy E(MS), a quantum chemical descriptor of the active TMS phases [10–12]. This kinetic modeling has also shown that the optimum of selectivity corresponds to the CoMoS catalyst. However, in specific conditions, it appears that it is possible to modulate the HDS/HydO selectivity of the NiMoS [4,9] and CoMoS [8] active phases. Hence, for an improved understanding on the nature of Co(Ni)MoS active sites involved in the HDS/HydO selectivity, an atomistic description of the reactivity of olefins derivatives is mandatory.

Numerous experimental [13–16] and theoretical works [17–23] have provided an atomistic description of the Co(Ni)MoS active phases. Recent first principles molecular modeling [18], based on the density functional theory (DFT) has underlined that the change of morphology together with the promoter content of the Co(Ni)MoS nano-crystallites as a function of sulfo-reductive reaction conditions may be viewed as a manifestation of the Le Chatelier's principle. DFT calculations [17–19] and scanning tunneling microscopy (STM) [13,14] have thus provided a quantitative determination of the 2D deformed hexagonal morphology of Co(Ni)MoS nano-crystallites. Co(Ni)MoS nano-crystallites exhibit MoS_2 slabs presenting two different edges, called M-edge and S-edge [24]. Promoter atoms (Co, Ni) are located in substitution of Mo atoms at the edges [14,15,25,26]. The sulfur and promoter contents vary with reaction conditions, simultaneously changing the edge energies and the 2D-morphology of these crystallites [14,17,18]. As a consequence, the nature of the active edge and its sulfur coverage vary as a function of reaction conditions. Whereas the edges expose only promoter atoms in highly sulfiding conditions, se-

* Corresponding author at: IFP, Direction Catalyse et Séparation, Rond-Point de l'Échangeur de Solaize, BP 3, 69360 Solaize, France. Fax: +33 4 78 02 20 66.
E-mail address: pascal.raybaud@ifp.fr (P. Raybaud).

0021-9517/$ – see front matter
doi:10.1016/j.jcat.2008.09.026

vere reductive conditions induce a segregation of the promoter atoms from the edges. Intermediately, in HDS reaction conditions, Co(Ni)MoS active phases have been found to exhibit different behavior: whereas both NiMoS edges may be totally or partially promoted, the CoMoS S-edge will be totally promoted and its M-edge only partially promoted by Co.

Many DFT works have also performed adsorption energy calculations of sulfur organic molecules including thiophene and dibenzothiophene [27–33] and nitrogen organic molecules [20,34,35]. The mechanism of thiophene and thiols HDS on MoS_2 was also investigated in recent DFT studies [36,37]. These various works highlight the different chemical behaviors of the two edges with respect to the molecules adsorption and activation process. However, to our knowledge, no DFT work was devoted to the theoretical investigation of olefins adsorption on CoMoS and NiMoS model catalysts in sulfo-reductive conditions. Thus, it appears that the DFT calculation of the thermodynamic stability of relevant olefins on Co(Ni)MoS catalysts in H_2S/H_2 conditions is mandatory to provide a better understanding of HDS/HydO selectivity trends.

The present work focuses on the DFT calculation of the adsorption energies and configurations of two relevant model molecules for HDS (2MT) and HydO (23DMB1N) reactions on the Co and Ni promoted M- and S-edges stable in reaction conditions. An exhaustive investigation of the adsorption modes is undertaken on the relevant Co(Ni)Mo active sites determined in our recent work [18]. The main objective of this work is to explore the effect of the promoter (i.e. nature and content) and of the type of promoted edge (i.e. morphology effect) on the selective adsorption of FCC gasoline model molecules in reaction conditions. An interpretation of the HDS/HydO selectivity observed experimentally will be proposed by combining our DFT results and recent kinetic modeling.

In the following section, we present the methodology used for the calculation of edge energies in presence of adsorbed molecules as a function of reaction conditions. We also describe the adsorption modes investigated for both model molecules. In Section 3, the energy results (i.e. adsorption energies) are presented for CoMoS and NiMoS respectively, and an electronic analysis is provided. The discussion is devoted to the extrapolation of the energy results to realistic reaction conditions and to the interpretation of the recently established kinetic modeling of HDS/HydO selectivity [3,9].

2. Methods

2.1. Edge energy calculation

The total energy calculations are based on the plane wave density functional theory within the generalized gradient approximation [38,39]. In line with our previous works [17–19], we used the Vienna ab-initio simulation package [40,41] to solve the Kohn–Sham equations [42,43] within the projected augmented wave formalism [44]. The cut-off energy governing the size of the plane wave basis set is fixed at 500.0 eV. The geometry optimization is completed when the convergence criteria on forces becomes smaller than 0.05 eV/Å.

As mentioned in introduction, our previous study had explored the promoter contents of the edges as a function of reaction conditions [18]. From these results, morphology diagrams have been constructed for Co(Ni)MoS nano-crystallites. The main objective of this work is to investigate the competitive adsorption between two relevant HDS and HydO model reactants, which have been chosen consistently with the previous experimental and kinetic modeling works [3,9]. The gasoline produced by the FCC process is mainly composed of aromatics, isoalkenes and alkylthiophenes. As a consequence, a relevant model molecule for the HDS reaction is 2-methylthiophene (called 2MT), and a relevant olefin for HydO is 2,3-dimethylbut-1-ene (called 23DMB1N) known to be produced by the fast isomerization of the 2,3-dimethyl-but-2-ene (23DMB2N) on the alumina support [5,6].

Taking advantage of our previous DFT results [18], the effects of the promoter content, sulfur coverage and of the type of edge on this competitive adsorption are investigated, considering the stable edges in sulfo-reductive conditions. The stable adsorption modes of the two molecules have also been taken into account.

Based on our previous DFT investigations [17–19], the absolute energies of the M- and S-edges calculated therein are used as energy reference. Periodic supercells have been chosen consistently with our last study [18]. In the $z(z')$ direction (Fig. 1), the slab contains four Mo sub-surface layer capped by one row of metal-

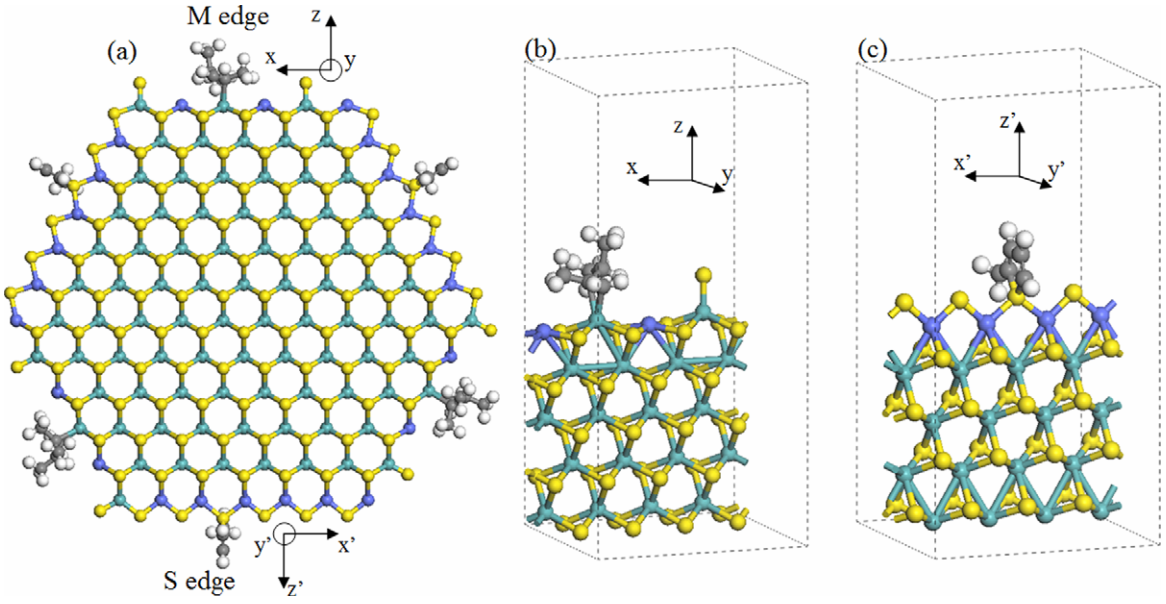

Fig. 1. Periodic slabs used to simulate molecules adsorption on M- and S-edges of a promoted MeMoS nano-crystallite (a) with various promoter (Me) contents. The stoichiometry of the slab ($Mo_xMe_yS_z$–Mol) depends on the S-coverage (z) and on the (Me) promoter content (y); (b) example of a partially promoted M-edge with an adsorbed 23DMB1N; (c) example of a fully promoted S-edge with an adsorbed 2MT; (yellow balls: S, green balls: Me = Mo, blue balls: Co or Ni, gray balls: C, white balls: H.) (For interpretation of the references to color in this figure legend, the reader is referred to the web version of this article.)

lic atoms (Mo and/or Co or Ni). In the $x(x')$ direction, four edge sites are considered. According to our previous DFT calculations [18,24,26], the corresponding cell parameters (12.29 Å, 12.80 Å, 27.00 Å) ensure a vacuum interlayer of more than 10 Å in the $z(z')$ direction and more than 6 Å in the $y(y')$ direction. The k-point mesh $(3, 3, 1)$ is also optimized to ensure an accurate discrete sampling of the supercell's Brillouin zone with a Methfessel and Paxton smearing method (order 1 and sigma = 0.1). Dipole corrections have been applied to each cell, due the non-symmetric slab.

Determining the stable adsorption modes of both molecules adsorbed on both edges in reaction conditions requires the calculation of the edge energies with the adsorbed molecules in various configurations and for different sulfur coverages and promoter contents. As shown in [17,19,24,26], the sulfur coverage and promoter (Me) content at the edge depends on the sulfo-reductive conditions fixed by the temperature and $p(H_2S)/p(H_2)$ ratio. One way to solve this problem using periodic slabs is to calculate the edge energy with the adsorbed molecule using the following chemical equation:

$$x\mathrm{MoS}_a|_{\mathrm{bulk}} + \frac{y}{b}\mathrm{Me}_b\mathrm{S}_c|_{\mathrm{bulk}} + \left(z - xa - \frac{yc}{b}\right)\mathrm{H_2S} + \mathrm{Mol} \rightarrow \mathrm{Mo}_x\mathrm{Me}_y\mathrm{S}_z - \mathrm{Mol}|_{\mathrm{edge}} + \left(z - xa - \frac{yc}{b}\right)\mathrm{H_2}, \quad (1)$$

where MoS_a ($\mathrm{MoS_2}$ or Mo) and $\mathrm{Me}_b\mathrm{S}_c$ ($\mathrm{Co_9S_8}$, Co, $\mathrm{Ni_3S_2}$, Ni) represent the reference sulfide or metallic bulk phases, stable in reaction conditions. Mol is the corresponding molecule (2MT or 23DMB1N) in gaz phase, and $\mathrm{Mo}_x\mathrm{Me}_y\mathrm{S}_z$–Mol is the global stoichiometry of the slab supercell used for the promoted M- and S-edge with the molecule adsorbed on it (Figs. 1b–1c). The supercell exhibiting four non-equivalent edge sites, with y atoms of promoter (Me), the total number of Mo atoms, is equal to $x = 20 - y$, the total number of sulfur atoms (excluding 2MT) is equal to z.

The variation of the free energy for the promoted M-edge with the adsorbed molecule is written as follows:

$$\Delta G_{M\text{-edge}}(\Delta\mu_S, \mathrm{Mol}) = \Delta G_{M\text{-edge}}(\Delta\mu_S) + \Delta G_{\mathrm{ads}}(\mathrm{Mol}). \quad (2)$$

In the same spirit as in our previous studies [17,18], $\Delta G_{M\text{-edge}}$ is expressed as follows:

$$\Delta G_{M\text{-edge}}(\Delta\mu_S) \approx E(\mathrm{Mo}_x\mathrm{Me}_y\mathrm{S}_z)_{M\text{-edge}} - xE(\mathrm{MoS}_a) - \frac{y}{b}E(\mathrm{Me}_b\mathrm{S}_c) - \left(z - xa - \frac{yc}{b}\right)\left(\Delta\mu_S + E(\mathrm{S}_\alpha)\right). \quad (3)$$

The variation of the chemical potential of sulfur as a function of T and $p_{\mathrm{H_2S}}/p_{\mathrm{H_2}}$ is given by the following expression [20,45]:

$$\Delta\mu_S = h_{\mathrm{H_2S}}(T) - h_{\mathrm{H_2}}(T) - E_{\mathrm{S}_\alpha} - T\left[s_{\mathrm{H_2S}}(T) - s_{\mathrm{H_2}}(T)\right] + RT\ln(p_{\mathrm{H_2S}}/p_{\mathrm{H_2}}). \quad (4)$$

The numerical values of $\Delta\mu_S$ are also reported on the abacus of Refs. [20,45].

Neglecting the variation of the pV terms during adsorption and assuming same partial pressures of 2MT and 23DMB1N, the free energy of adsorption is expressed as follows, where Z represents the one-particle partition functions of indistinguishable particles:

$$\Delta G_{\mathrm{ads}}(\mathrm{Mol}) = \Delta E_{\mathrm{ads}}(\mathrm{Mol}) - RT\ln\left(\frac{Z_{\mathrm{ads}}}{Z_{\mathrm{gas}}}\right). \quad (5)$$

The adsorption energy is given by the following expression:

$$\Delta E_{\mathrm{ads}}(\mathrm{Mol}) = E(\mathrm{Mo}_x\mathrm{Me}_y\mathrm{S}_z - \mathrm{Mol}) - E(\mathrm{Mo}_x\mathrm{Me}_y\mathrm{S}_z) - E(\mathrm{Mol}), \quad (6)$$

where $E(\mathrm{Mo}_x\mathrm{Me}_y\mathrm{S}_z$–Mol) is the energy of the molecule adsorbed on the edge with the $\mathrm{Mo}_x\mathrm{Me}_y\mathrm{S}_z$ composition, $E(\mathrm{Mol})$ is the energy of the isolated molecule at 0 K and $E(\mathrm{Mo}_x\mathrm{Me}_y\mathrm{S}_z)$ the energy of the same edge.

For the adsorbed molecule, the contribution of the rotational and translational contributions are transformed in additional vibrational contribution, i.e. $Z_{\mathrm{ads}} = Z_{\mathrm{ads}}(\mathrm{vib})$. The marginal difference between the zero-point energy correction for the free and adsorbed molecule allows us to neglect this contribution. The same assumption is made for the vibrational contributions. We have tested these assumptions in the case of two relevant adsorption configurations of the 2MT molecule showing that the energy correction would be less than 0.02 eV/edge atom. We thus obtain the following expression:

$$\Delta G_{\mathrm{ads}} = \Delta E_{\mathrm{ads}} - RT\ln\left(\frac{Z_{\mathrm{ads}}(\mathrm{vib})}{Z_{\mathrm{gas}}(\mathrm{rot})Z_{\mathrm{gas}}(\mathrm{trans})Z_{\mathrm{gas}}(\mathrm{vib})}\right) \approx \Delta E_{\mathrm{ads}} - RT\ln\left(\frac{1}{Z_{\mathrm{gas}}(\mathrm{rot})Z_{\mathrm{gas}}(\mathrm{trans})}\right). \quad (7)$$

Similar approximations have been previously proposed for the adsorption of small molecules on metallic systems [46], confirming that rotational and translational entropy are the predominant sources of entropy loss during adsorption.

The slabs representing the $\mathrm{Mo}_x\mathrm{Me}_y\mathrm{S}_z$–Mol edges expose simultaneously both edges: the promoted M-edge (with various promoter content and adsorbed molecules) at the top, and the non-promoted S-edge (with 100% S) at the bottom (Fig. 1b). Symmetrically, the second type of slab (Fig. 1c) contains the promoted S-edge (with various promoter content and molecules) at the top and the non-promoted M-edge (0% S) at the bottom. Hence, the edge energy value of the top edge (the promoted M-edge with an adsorbed molecule, for example) can be calculated only if the edge energy (depending on $\Delta\mu_S$) of the bottom edge (the non-promoted S-edge with 100% S in our example) is known. Such edge energies, calculated in [19] are taken into account. In case of M-edge, this leads to the following expression:

$$\sigma_{M\text{-edge}}(x, z, \Delta\mu_S, \mathrm{Mol}) = \frac{1}{4}\Delta G_{M\text{-edge}}(x, z, \Delta\mu_S, \mathrm{Mol}) - \sigma_{S\text{-edge}}(y = 0,\ z = 100\%\ S,\ \Delta\mu_S) \quad (8)$$

where $\sigma_{S\text{-edge}}$ ($y = 0$, $z = 100\%$ S, $\Delta\mu_S$) represents the edge energy value of the non-promoted S-edge ($y = 0$) exposed at the bottom of the slab with z value corresponding to 100% S coverage (the value is taken from [19]).

An equivalent expression is used for the S-edge:

$$\sigma_{S\text{-edge}}(x, z, \Delta\mu_S, \mathrm{Mol}) = \frac{1}{4}\Delta G_{S\text{-edge}}(x, z, \Delta\mu_S, \mathrm{Mol}) - \sigma_{M\text{-edge}}(y = 0,\ z = 0\%\ \mathrm{S},\ \Delta\mu_S), \quad (9)$$

where $\sigma_{M\text{-edge}}$ ($y = 0$, $z = 0\%$ S, $\Delta\mu_S$) represents the edge energy value [19] of the non-promoted M-edge ($y = 0$) exposed at the bottom of the slab with z value corresponding to 0% S coverage.

In Eqs. (8) and (9), the edge energies with adsorbed molecules not only depend on T and $p(H_2S)/p(H_2)$, but also on the promoter edge content (y), on the S-coverage (z), and on the type of molecule adsorbed (Mol). These equations will be used to plot the edge energies diagram in the Section 4.

Finally, the adsorption selectivity (adsorption competition) will be quantified by the $\Delta\sigma_{\mathrm{edge}}$ index, evaluating the difference of the edge energies for the two adsorbed molecules (2MT and 23DMB1N):

$$\Delta\sigma_{\mathrm{edge}} = \sigma_{\mathrm{edge}}(2\mathrm{MT}) - \sigma_{\mathrm{edge}}(23\mathrm{DMB1N}). \quad (10)$$

A negative value of $\Delta\sigma_{\mathrm{edge}}$ indicates a selective adsorption of 2MT versus 23DMB1N, i.e. a stronger affinity of 2MT for the edge. It can be noticed that the variation of $\Delta\sigma_{\mathrm{edge}}$ is mainly tuned by $\Delta E_{\mathrm{ads}}(2\mathrm{MT}) - \Delta E_{\mathrm{ads}}(23\mathrm{DMB1N})$. The $\Delta\mu_S$ term may also impact

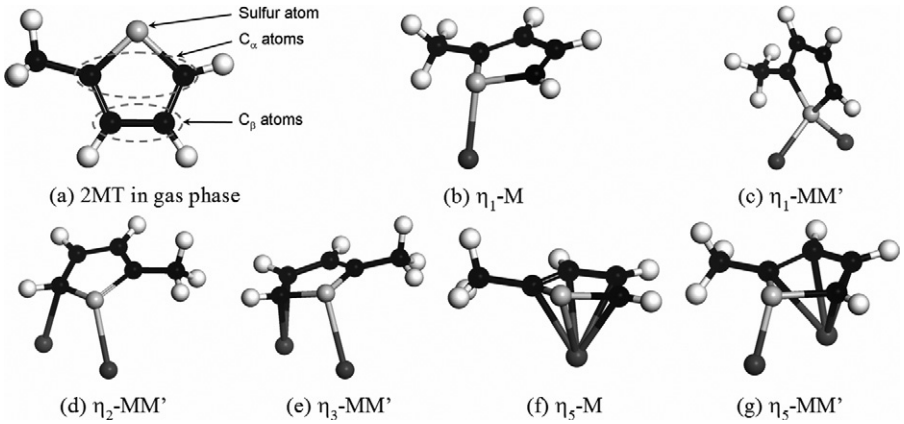

Fig. 2. Simplified representation of the adsorption modes of 2MT. (Black balls: C, White balls: H, Dark gray balls: edge site (Mo, Co or Ni), Light gray balls: S).

the $\Delta\sigma_{edge}$ index, if different sulfur coverages or promoter contents are stabilized in presence of the adsorbed molecules. In contrast, the contribution of the partition functions of the two molecules will compensate, leading to a negligible contribution of the two terms $-RT\ln(\frac{Z_{ads}}{Z_{gas}})$ in $\Delta\sigma_{edge}$.

According to our previous work [18], for the CoMoS model used, the y value will be equal to 50 or 100% on the M-edge, corresponding to a partial or a full edge promotion. In the case of the partial promotion, the paired –Co–Co–Mo–Mo– and alternated –Co–Mo–Co–Mo– configurations will be considered, with 25% S. The fully promoted edge sulfur coverage varies from 0 to 50% S. On S-edge, only the fully promoted edge ($y = 100\%$ S) is considered, with 50% S to 75% S. For NiMoS, the y value will be equal to 50% or 100% on both M- and S-edges. The partially promoted M-edge will be covered by 12.5% S while the fully promoted M-edge sulfur coverage varies from 0% to 50% S. On the S-edge, the sulfur coverage is equal to 50% S for both promoters content. In every case, lower sulfur coverages (12.5% S less) will also be investigated, considering the removal from a sulfur atom by molecules adsorption. In the same spirit, too high sulfur coverage will not be investigated: 50% S and more for the M-edge and more than 62.5% S on the S-edge.

2.2. Adsorption modes

Different adsorption modes of 2MT have been investigated on the two edges (Fig. 2). They are noted η_i-MM′, where i stands for the number of atoms of 2MT assumed to be bonded to metal site (M and/or M′ = Mo, Co or Ni) belonging to the M- or S-edge. The sulfur atom of the molecule is always bonded to the first metal site (M).

(b) η_1-M: the molecule interacts by its S atom on top of one metal site (M).
(c) η_1-MM′: the molecule interacts by its S atom in a bridging position between two neighboring metal sites (M and M′).
(d) η_2-MM′: the molecule interacts by the S atom to one metal site (M), and by one C_α atom to one neighboring metal sites (M′).
(e) η_3-MM′: the molecule interacts by the S atom to one metal site (M), and by one C_α and one C_β atom to another metal site (M′).
(f) η_5-M: the molecule interacts by all atoms belonging to the aromatic ring to one metal site (M).
(g) η_5-MM′: the molecule interacts by the S atom to one metal site (M), and by all its C aromatic atoms to the same metal site (M) or to one neighboring metal site (M′).

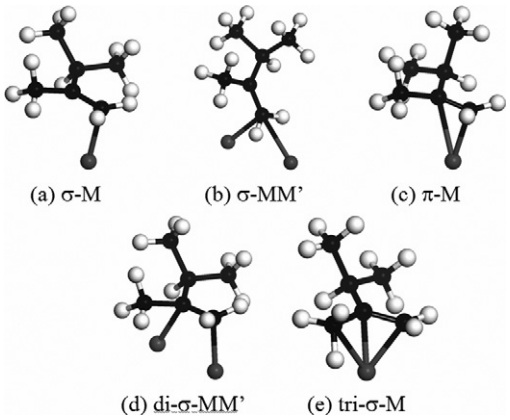

Fig. 3. Simplified representation of the adsorption modes of 23DMB1N. (Black balls: C, White balls: H, Dark gray balls: edge site (Mo, Co or Ni)).

Different adsorption modes have also been investigated for the 23DMB1N on both edges (Fig. 3):

(a) σ-M: the molecule interacts by one C atom of the C=C bond to one metal site (M).
(b) σ-MM′: the molecule interacts by one C atom of the C=C bond to two metal sites (M and M′).
(c) π-M: the molecule interacts by the C=C double bond to one metal site (M).
(d) di-σ-MM′: the molecule interacts by each C of the C=C double bond to two metal sites (M and M′).
(e) tri-σ-M: the molecule interacts by the C=C double bond and by the methyl C_α atom to one metal site (M).

For both molecules adsorbed on the different types of edges, we have simulated about 180 different configurations. For sake of clarity, only the most relevant configurations are reported in what follows.

2.3. Electronic analysis of the chemical bonding

In order to provide quantitative analysis at the electronic level on the bonding between molecules and edges, the topological analysis of some adsorption configurations have been carried out. To make this analysis, we choose the electron localization function (ELF) [47–50], which provides a description close to Lewis' description of chemical bonding [51,52].

In practical, from periodic cells' optimized geometries, we construct clusters representative of the adsorption configuration. B3LYP calculations [53,54] are performed on these clusters, with

Table 1
Adsorption energies of the stable 2MT configurations on the CoMoS M-edge (see Fig. 4 for the atomic structures).

Promoter (%)	S (%)	Adsorption configuration	ΔE_{ads} (eV)
50% alt	25.0%	η_2-CoMo 1A	−0.54
	12.5%	η_5-CoMo 1B	−2.31
50% pair	25.0%	η_3-CoCo 1C	−0.97
		η_3-MoCo 1D	−0.90
	12.5%	η_3-CoCo 1E	−1.19
100%	37.5%	η_3-CoCo 1F	−0.37
	25.0%	η_3-CoCo 1G	−1.12
	12.5%	η_3-CoCo 1H	−1.21
	0.0%	η_3-CoCo 1I	−1.30

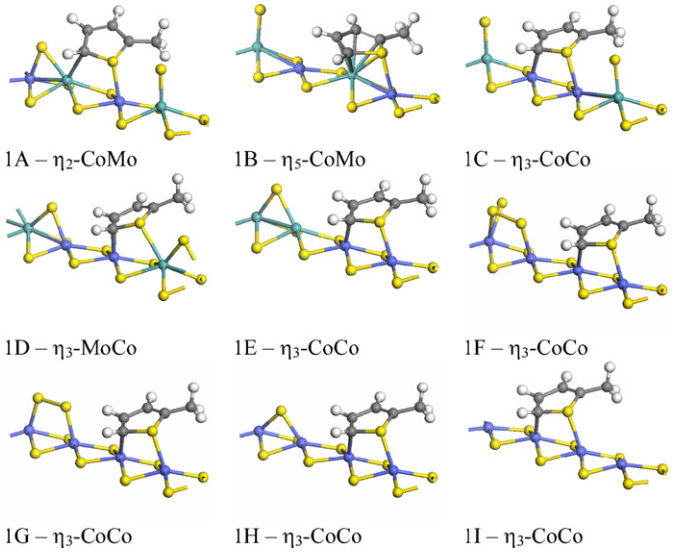

Fig. 4. Stable 2MT adsorption configurations on CoMoS M-edge (see Table 1 for energy values). Same color legend as in Fig. 1. (For interpretation of the references to color in this figure legend, the reader is referred to the web version of this article.)

the standard 3-21G basis set [55], using the Gaussian 03 software [56].

A trick is used to reduce the size of the output wavefunctions, which are then analyzed using the TopMoD program [57,58]. This program calculates the ELF values on a grid and then provides its analysis using the dynamical system theory [59,60]. The ELF isosurfaces have then been visualized with the Amira 3.0 software [61]. The accuracy of the integrated densities remains within the order of 0.02*e* (electrons).

3. Results

3.1. Case of the CoMoS

3.1.1. Adsorption on the M-edge

2-Methylthiophene (2MT) Table 1 indicates the most stable adsorption energies and their configurations are represented in Fig. 4. We first observe that the stable adsorption and energies depends both on the promoter edge content and on the sulfur coverage. Indeed, the most exothermic configurations on mixed sites (50% Co) are presenting sulfur species strongly linked to the M-edge sites (which was also the case of the stable edge without molecule). The sulfur species cannot be displaced by the 2MT molecule which consequently interacts with the remaining free sites. On mixed sites with 25% S, the most stable adsorption is found for the pairing –Mo–Co–Co–Mo– edges (1C, 1D) rather than the alternated –Mo–Co–Co–Mo– ones (1A). The pairing configuration with S top linked to Mo implies that the adjacent free sites can adsorb the molecule in η_3 mode. In contrast, the alternated one requires a displacement of the S atoms in a bridging position to enable the molecule adsorption in a η_2 mode.

On the edge with mixed sites and 12.5% S, we observe that contrary to the pairing edge (1E), the most exothermic adsorption on the alternated edge (1B) occurs with the η_5-CoMo mode. This configuration has not been observed before because it requires one Mo free site to interact with the aromatic ring of the molecule. For other edges, this configuration requires a too energy demanding S displacement. In general, the 12.5% S adsorption configurations are more exothermic than the 25% S ones, meaning that increasing the S-coverage (as induced by $p(H_2S)$) destabilizes the 2MT molecule. On the totally promoted edge, with low sulfur content (1G–1I), the adsorption of the molecule is as exothermic as on the pairing 12.5% S mixed edge (1E), which are presenting exactly the same configuration. At higher sulfur content (1F), because of steric repulsion between S and 2MT, the organization of the S atoms at the edge costs too much energy, which implies a less exothermic adsorption.

Table 2
Adsorption energies of the stable 23DMB1N configurations on the CoMoS M-edge (see Fig. 5 the atomic structures).

Promoter (%)	S (%)	Adsorption configuration	ΔE_{ads} (eV)
50% alt	25.0%	σ-Co 2A	−0.08
	12.5%	π-Mo 2B	−1.54
50% pair	25.0%	σ-Co 2C	−0.43
	12.5%	π-Co 2D	−0.72
100%	37.5%	σ-Co 2E	−0.19
	25.0%	π-Co 2F	−0.73
	12.5%	π-Co 2G	−0.74
	0.0%	π-Co 2H	−0.79

2,3-Dimethylbut-1-ene (23DMB1N) Table 2 and Fig. 5 report the most stable adsorption configurations of 23DMB1N and the corresponding adsorption energies. As noticed for 2MT, the position of sulfur atoms at the edge also strongly influences the adsorption configurations of the molecule. Since Mo presents a higher affinity for S than for C, the unique edge configuration stabilizing the π-Mo adsorption (2B) is the mixed alternated edge with 12.5% S. For all other edges the most exothermic adsorption modes is π-Co or σ-Co, whereas S atoms inhibit the Mo sites.

On the Co sites, the olefin adsorption is always more exothermic on the edges with low S content (2D, 2F-H) than with higher S content (2A, 2C, 2E). Furthermore, the adsorption energies of the 23DMB1N are always significantly weaker than the 2MT ones: it comprises between −0.18 and −0.77 eV, whereas for 2MT the values comprises between −0.37 and −2.31 eV. This result implies that when both molecules compete for the same site on the CoMoS M-edge, 2MT is adsorbed preferentially to 23DMB1N and inhibits the olefin hydrogenation, as also suggested in [7].

Comparison with H_2 If one compares with adsorption energies of H_2 reported in the literature [22,62], the most favorable adsorption energy of H_2 is about −0.55 for the heterolytic dissociation on Co-S pair of the CoMoS M-edge. The effect of H_2 on the adsorption modes found for 2MT and 23DMB1N on the promoted M-edge is thus expected to remain modest due to their stronger adsorption energies (except for the configurations 2A and 2C of 23DMB1N).

ELF analysis To explain this energy trend, we provide an ELF analysis of the most favored adsorption modes of both molecules on the paired edge with 12.5% S (Fig. 6). For the (1E) adsorption mode of 2MT, we observe the creation of three bonding basins between

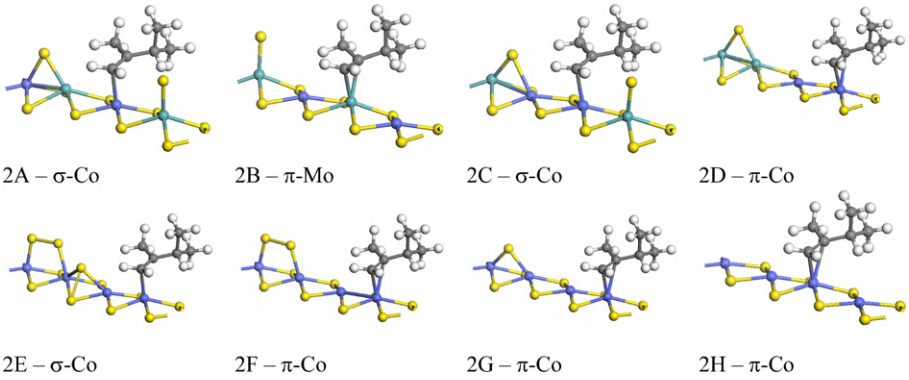

Fig. 5. Stable 23DMB1N adsorption configurations on CoMoS M-edge (see Table 2 for energy values). Same color legend as in Fig. 1. (For interpretation of the references to color in this figure legend, the reader is referred to the web version of this article.)

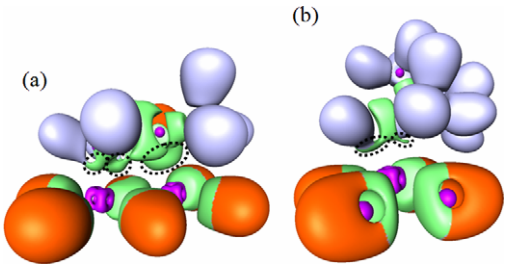

Fig. 6. (a) ELF = 0.7 localization domains of 2MT adsorbed in η_3 mode on Co–Co sites (1E); (b) ELF = 0.7 localization domains of 23DMB1N adsorbed in π mode on a Co site (2D); dotted circles indicate the bonding basins between the molecule and the edge.

Table 3
Adsorption energies of the stable 2MT configurations on the CoMoS S-edge (see Fig. 7 the atomic structures).

Promoter (%)	S (%)	Adsorption configuration	ΔE_{ads} (eV)
100%	62.5%	η_1-CoCo 3A	−0.22
	50.0%	η_1-CoCo 3B	−0.24
	37.5%	η_1-CoCo 3C	−1.39
		η_5-CoCo 3D	−1.37

the 2MT and the edge, in support of the "η_3 mode" denomination. Similarly, for the (2D) adsorption mode of the olefin, we observe the creation of two bonding basins between the 23DMB1N and the edge, in accordance with the "π mode" labeling. The quantification of the total basins population shows that it is 1.01*e* for the two C–Co 23DMB1N basins, 4.20*e* for the three 2MT basins including 2.26*e* for the S·Co basin, and 1.94*e* for the two C–Co basins. This corroborates the previous energy results: 2MT interacts more strongly with the edge site than 23DMB1N, creating more bonding basins, with a higher population. Furthermore, the S–Co bonding plays a key contribution in this interaction.

3.1.2. Adsorption on the S-edge

2-Methylthiophene (2MT) The most stable adsorption configurations of 2MT are shown in Fig. 7 and their respective adsorption energies reported in Table 3.

A great majority of the stable adsorption mode of 2MT are η_1-CoCo trough the S atom (3A–3C). The sole highly coordinated and exothermic configuration is a η_5-CoCo mode, observed for a less S-covered edge (37.5% S–3D). This implies, as observed previously on the M-edge, that the position of the sulfur atoms at the edge is of major importance for the molecule adsorption. We also observe that adsorption on a less sulfided edge (3C, 3D) is more exothermic that on more sulfided edges (3A, 3B), by about 1.1 eV.

2,3-Dimethylbut-1-ene (23DMB1N) The stable adsorption configurations and their adsorption energies are presented in Fig. 8 and Table 4. A significant distinction between 2MT and 23DMB1N adsorption on the Co fully promoted S-edge is observed: on highly sulfided edges (4A, 4B), 23DMB1N has never been found to be exothermically adsorbed, whereas it exhibits an exothermic adsorption energy of −0.51 eV only on the strongly sulfur depleted edge (4C). As observed for 2MT on the same edges, this results from a highly coordinated adsorption mode (tri-σ, 4C) only achievable on the less S-covered edge (37.5% S). Such a configuration is about 1.2 eV more stable than less coordinated one (σ-CoCo, 4A, 4B). However, such low S-coverage reaction conditions cannot be reached in realistic HDS conditions (as discussed later).

Comparing 23DMB1N and 2MT adsorption on the CoMoS S-edge, we first note that for similar edge configurations, 2MT is favorably adsorbed by about 0.9 eV. This induces that if both molecules compete for adsorption on this edge, 2MT will be significantly more strongly adsorbed. As for the M-edge, this favored adsorption of 2MT versus 23DMB1N is due to the presence of the S atom, interacting trough its lone pair electrons with Lewis metallic sites. When 23DMB1N adsorbs, the π electrons involved in the C=C double bond cannot interact so easily with the Co site at the edge. Only if a low S coordination of the Co site exists, 23DMB1N exhibits exothermic adsorption energy.

Comparison with H_2 Comparing again with H_2 adsorption energies reported in the study by Sun et al. [63], it appears that the most favorable adsorption energy of H_2 is about −0.87 eV for its

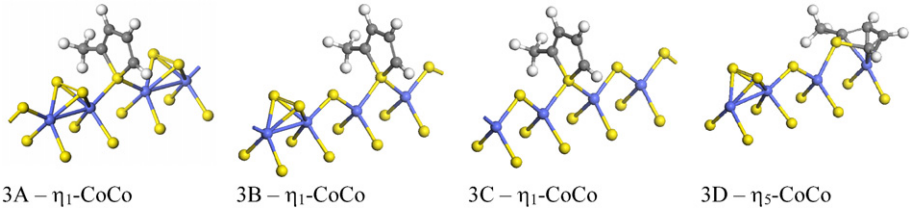

Fig. 7. Stable 2MT adsorption configurations on CoMoS S-edge (see Table 3 for energy values). Same color legend as in Fig. 1. (For interpretation of the references to color in this figure legend, the reader is referred to the web version of this article.)

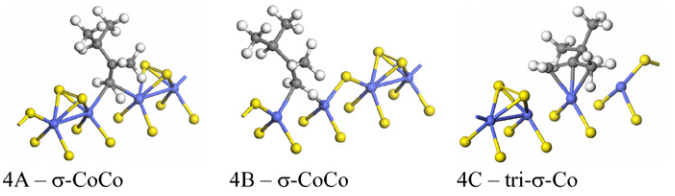

Fig. 8. Stable 23DMB1N adsorption configurations on CoMoS S-edge (see Table 4 for energy values). Same color legend as in Fig. 1. (For interpretation of the references to color in this figure legend, the reader is referred to the web version of this article.)

Table 4
Adsorption energies of the stable 23DMB1N configurations on the CoMoS S-edge (see Fig. 8 for the atomic structures).

Promoter (%)	S (%)	Adsorption configuration	ΔE_{ads} (eV)
100%	62.5%	σ-CoCo 4A	+0.68
	50.0%	σ-CoCo 4B	+0.72
	37.5%	tri-σ-Co 4C	−0.51

Table 5
Adsorption energies of the stable 2MT configurations on the NiMoS M-edge (see Fig. 9 for the atomic structures).

Promoter (%)	S (%)	Adsorption configuration	ΔE_{ads} (eV)
50% pair	12.5%	η_2-MoNi 5A	−0.26
		η_1-Ni 5B	−0.23
	0.0%	η_5-MoMo 5C	−2.90
100%	0.0%	η_1-Ni 5D	−0.51
		η_2-NiNi 5E	−0.45

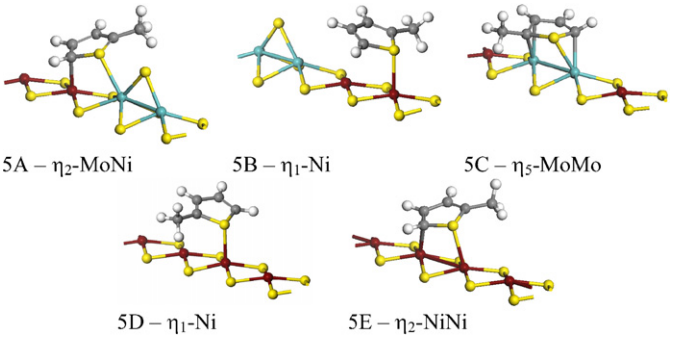

Fig. 9. Stable 2MT adsorption configurations on NiMoS M-edge (see Table 5 for energy values). (Yellow balls: S, green balls: Mo, brawn balls: Ni, gray balls: C, white balls: H). (For interpretation of the references to color in this figure legend, the reader is referred to the web version of this article.)

homolytic dissociation, leading to two S–H groups on the CoMoS S-edge. It can be thus deduced that H_2 may exhibit adsorption energies as high as some configurations of 2MT (3A and 3B) and even higher than 23DMB1N.

3.2. Case of the NiMoS

3.2.1. Adsorption on M-edge

2-Methylthiophene (2MT) Table 5 indicates the adsorption energy of the most stable adsorption mode, and Fig. 9, their corresponding atomic structures. The stable mixed edges presenting 12.5% S is more stable in the pairing configuration than in the alternated one, which implies that the edge is less sterically hindered by S atoms and more accessible to the molecule. As a consequence, 2MT adsorption is less dependent on the position of the S covering atom than in the CoMoS case. For the configuration (5A), where 2MT adsorbs in a η_2-MoNi mode, sharing one Mo site with a covering S atom, the energy competes with the less coordinated η_1-Ni configuration (5B). As a consequence, this lower sulfur coverage—compared to CoMoS—makes free Mo–Mo sites available to adsorb the molecule. This results on the highly coordinated η_5-MoMo adsorption configuration (5C), presenting a highly exothermic adsorption.

Regarding the totally promoted edge, the most exothermic η_1-Ni adsorption (5D) has not been observed before. We also observe a competitive exothermic η_2-NiNi configuration (5E), close to the values reported for thiophene by Sun et al. [31]. This η_1-Ni configuration (5D) is due to the weaker Ni–C(sp^2) interaction compared to Co–C(sp^2). This is confirmed when comparing adsorption energy for similar configurations on NiMoS and on CoMoS (5A vs 1D): adsorption on NiMoS is about 0.65 eV less exothermic than on CoMoS.

Table 6
Adsorption energies of the stable 23DMB1N configurations on the NiMoS M-edge (see Fig. 10 for the atomic structures).

Promoter (%)	S (%)	Adsorption configuration	ΔE_{ads} (eV)
50% pair	12.5%	σ-Ni 6A	−0.13
	0.0%	di-σ-MoMo 6B	−1.94
100%	0.0%	σ-Ni 6C	−0.40

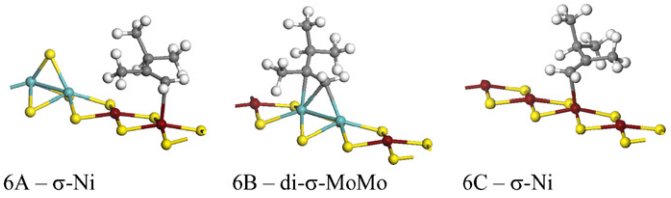

Fig. 10. Stable 23DMB1N adsorption configurations on NiMoS M-edge (see Table 6 for energy values). Same color legend as in Fig. 9. (For interpretation of the references to color in this figure legend, the reader is referred to the web version of this article.)

2,3-Dimethylbut-1-ene (23DMB1N) Table 6 and Fig. 10 give the energy and local structures of the most stable adsorption modes. As observed on CoMoS, only one edge configuration (6B) reveals an adsorption on Mo sites. Moreover, this configuration might be defined as a tri-σ-MoMo highly coordinated configuration, which is the most exothermic one on NiMoS. Except for this particular configuration, all σ-Ni modes (6A, 6C) are less stable than the equivalent on CoMoS (2C, 2H) by about 0.3 eV. This corroborates the preceding observation: the Ni–C σ-bond is weaker than the Co–C σ-bond.

Contrary to the case of CoMoS, the 2MT adsorption is not systematically favored versus the 23DMB1N adsorption. On the totally promoted edge, the difference in adsorption energies between 2MT and 23DMB1N is very narrow (0.05 eV), whereas on mixed sites, it is between 0.13 eV (12.5% S) and 0.96 eV (0% S). This competitive adsorption on the fully promoted edge implies that the two molecules may also compete for HDS and HydO on the same NiMoS site. On the other hand, molecules adsorption is less competitive on mixed sites, especially on the 0% S edge, leading to a higher affinity for 2MT than for 23DMB1N. This different situation observed for NiMoS compared to CoMoS is due to the weaker Ni–C bond than Co–C bond. Being less strong, Ni–C bond does not favor 23DMB1N adsorption, but also deserve 2MT adsorption, leading to a competitive situation on the fully promoted NiMoS M-edge. This result will be discussed in Section 4.

Comparison with H_2 According to [22], the adsorption of H_2 leads to the formation of H_2S on the S-atom present at the edge. The

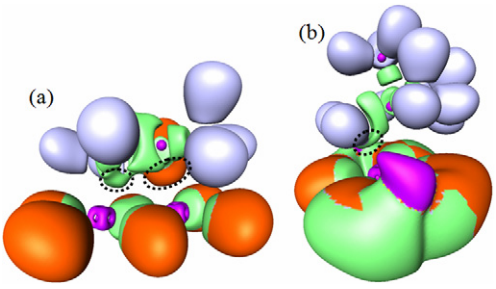

Fig. 11. ELF = 0.7 localization domains of (a) 2MT adsorbed in η_2 mode on the Ni–Ni sites (5D); (b) 23DMB1N adsorbed in σ mode on the Ni site (6C); dotted circles indicates the bonding basins between the molecule and the edge.

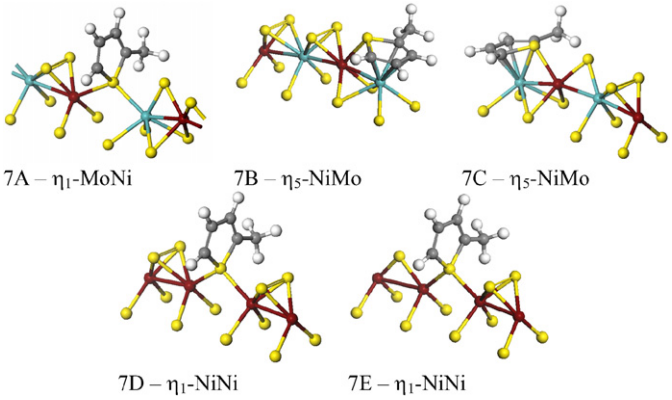

Fig. 12. Stable 2MT adsorption configurations on NiMoS S-edge (see Table 7 for energy values). Same color legend as in Fig. 9. (For interpretation of the references to color in this figure legend, the reader is referred to the web version of this article.)

corresponding adsorption energy (−0.5 eV) can thus reach those of 2MT and 23DMB1N.

ELF analysis To compare with the CoMoS M-edge, we provide the ELF analysis of the most favored adsorption modes of both molecules on the fully promoted edge with 0% S (Fig. 11).

For 2MT, two bonding basins are created between the 2MT and the edge for the (5D) mode, characterizing unambiguously the η_2 mode. A unique C–Ni bonding basin is evidenced between the 23DMB1N and the edge for the (6C) mode, in support of the σ mode. The quantification of these basins population indicates 0.64*e* for the 23DMB1N basin and 2.83*e* for the two 2MT basins, including 1.98*e* for the sole S–Ni basin. Comparing Co–C and Ni–C bonds, we note that the former populations (1.01*e* and 1.94*e* for 23DMB1N and 2MT) are always more important than the latter (0.64*e* and 0.85*e*, respectively), which confirms that the Ni–C bond is weaker than the Co–C bond. Furthermore, the slight difference in the Ni–C bonding population of both molecules (0.64*e* for 23DMB1N and 0.85*e* for 2MT) explains the small difference in adsorption energies between these two molecules. This result is also consistent with the higher difference in adsorption energy observed for CoMoS adsorption modes: an adsorption energy difference (between 23DMB1N and 2MT) of 0.47 eV corresponds to a carbon–promoter basin population difference of 0.93*e* for CoMoS versus respectively 0.05 eV and 0.21*e* for NiMoS modes.

3.2.2. Adsorption on the S-edge

2-Methylthiophene (2MT) 2MT adsorption on the NiMoS S-edge (Fig. 12) presents a more important variety of adsorption configurations, from low coordinated one to highly coordinated one. Whereas low coordinated adsorption configurations are observed on both mixed (7A) and the totally promoted edges (7D, 7E), highly coordinated adsorption configurations (7B, 7C) are only observed

Table 7
Adsorption energies of the stable 2MT configurations on the NiMoS S-edge (see Fig. 12 for the atomic structures).

Promoter (%)	S (%)	Adsorption configuration	ΔE_{ads} (eV)
50% alt	50.0%	η_1-MoNi 7A	+0.35
		η_5-NiMo 7B	+0.41
	37.5%	η_5-NiMo 7C	−1.29
100%	50.0%	η_1-NiNi 7D	−0.36
	37.5%	η_1-NiNi 7E	−0.59

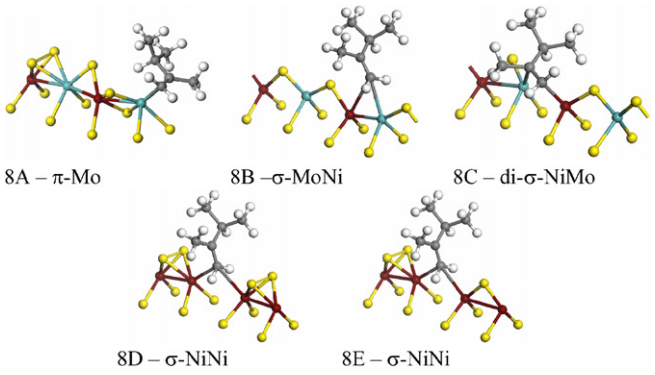

Fig. 13. Stable 23DMB1N adsorption configurations on NiMoS S-edge (see Table 8 for energy values). Same color legend as in Fig. 9. (For interpretation of the references to color in this figure legend, the reader is referred to the web version of this article.)

Table 8
Adsorption energies of the stable 23DMB1N configurations on the NiMoS S-edge (see Fig. 13 for the atomic structures).

Promoter (%)	S (%)	Adsorption configuration	ΔE_{ads} (eV)
50% alt	50.0%	π-Mo 8A	+0.81
	37.5%	σ-MoNi 8B	+0.14
		di-σ-NiMo 8C	+0.16
100%	50.0%	σ-NiNi 8D	+0.03
	37.5%	σ-NiNi 8E	−0.12

on the mixed edges. All adsorption configurations on the mixed edges require a small reconstruction of the edge, moving one Mo atom in a "M-edge like" position, linked to four S atoms of the sub-layer.

Considering the energy values (Table 7), we still observe a more exothermic adsorption on less S-covered edges (37.5% S) than on the more S-covered edge (50% S). Moreover, 2MT adsorption is more exothermic on the 37.5% S mixed edge than on the totally promoted edge, whereas its adsorption becomes endothermic on the 50% S mixed edge, contrary to the totally promoted edge with 50% S.

2,3-Dimethylbut-1-ene (23DMB1N) The most favorable adsorption configurations are presented in Fig. 13 and Table 8.

All adsorption configurations are low coordinated modes, except the di-σ-NiMo (8C) mode, observed on the mixed edge with 37.5% S. This configuration not observed on the edges with higher S-coverage is due to the steric effect of sulfur atoms at the edge. It is also not observed on the totally promoted edge, for similar steric reasons (8E).

While 23DMB1N adsorption on mixed sites (8A–8C) is always endothermic, its adsorption on the totally promoted edge is athermic with high S coverage (8D), or exothermic with lower S coverage (8E). Nevertheless, it is interesting to note that comparing the equivalently S-covered edges, 23DMB1N adsorption on the less S-

covered edges (37.5% S) is always more favorable by at least 0.15 eV than on the more S-covered edge (50% S).

Although 2MT adsorption on the mixed S-edge requires an edge reconstruction, it is more favored versus 23DMB1N on the mixed edge than on the totally promoted edge: the mixed edge favors 2MT versus 23DMB1N by at least 1.05 eV, whereas the fully promoted edge favors it up to 0.47 eV. The energy recovered by 2MT interaction compensates the edge energy reconstruction. Whatever the promoter edge content, a more favorable adsorption of 2MT versus 23DMB1N is thus revealed.

4. Discussion

In what follows, we discuss the relative stability of the two molecules in reaction conditions, by plotting the edge energy (σ_{edge}) of Co(Ni)MoS with the adsorbed molecules (according to Eqs. (7) and (8)), as a function of $\Delta\mu_S$ ($T = 523$ K, $p(H_2S)/p(H_2)$), T being fixed at 523 K, i.e. close to experimental conditions [3]. Figs. 14–17 represent the variation of σ_{edge} for the two molecules and the two promoter content on both the M- and S-edges. Hence, these diagrams consider the change of the promoter content and the sulfur coverage as a function of $p(H_2S)/p(H_2)$.

As the calculated 23DMB1N adsorption energy is never greater than 2MT—whatever the promoter and the edge considered—the edge energies of the adsorbed 23DMB1N (blue lines) are always greater than the one of 2MT (red lines). This implies that 2MT vs 23DMB1N adsorption selectivity index $\Delta\sigma_{edge}$ (as defined in Eq. (10)) is always negative.

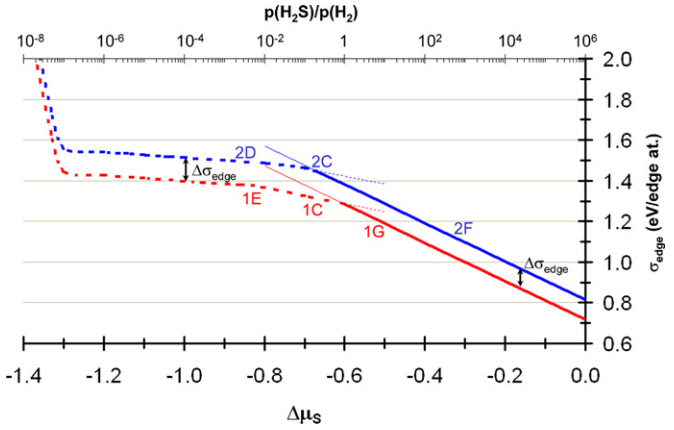

Fig. 14. Edge energy diagram of the molecules adsorbed on CoMoS M-edge as a function of $\Delta\mu_S$. The p_{H_2S}/p_{H_2} axis is determined for $T = 523$ K. (Blue line: 23DMB1N, red line: 2MT; full line: fully promoted edge; dashed line: partially promoted edge). (For interpretation of the references to color in this figure legend, the reader is referred to the web version of this article.)

4.1. CoMoS

The $\Delta\sigma_{M-edge}$ index of the M-edge, between −0.10 to −0.15 eV/edge atom (Fig. 14) shows that the selectivity between 2MT and 23DMB1N adsorption on the CoMoS M-edge is almost constant, whatever the value of $\Delta\mu_S$ (i.e. $p(H_2S)/p(H_2)$). This trend is explained by the fact that the term $\Delta E_{ads}(2MT) - \Delta E_{ads}(23DMB1N)$ does not depend drastically on the most stable configurations. In addition, the promoter content and the sulfur coverages of the two surfaces follows the same variation when the molecules are adsorbed. For the more sulfiding conditions, the configurations 1G for 2MT and 2F for 23DMB1N are stabilized. In both cases, the M-edge is fully promoted (solid lines) with a S-coverage of 25%. For more reductive conditions (dashed lines), the 1C, 1E configurations of 2MT and 2C, 2D configurations of 23DMB1N are stabilized. In these cases, the M-edge is partially promoted with a sulfur coverage of 25 or 12.5%. The smallest value of $\Delta\sigma_{edge}$ (−0.15 eV) is revealed at intermediate conditions where the 1C and 2C configurations are stabilized. Figs. 4 and 5 show that the 2MT molecule is able to displace one of the sulfur atom at the edge, whereas the 23DMB1N is more frustrated in the adsorbed state by the two neighboring S-atoms. It is also interesting that the slight minimum of $\Delta\sigma_{edge}$ is obtained in the case of partial promotion.

In the case of the CoMoS S-edge (Fig. 15), we also observe a constant selectivity index, however, it is smaller than the $\Delta\sigma_{M\text{-edge}}$ (−0.22 eV/edge atom). According to this value, it is suspected that the adsorption of 23DMB1N will be strongly inhibited by 2MT. On this edge, the fully promoted edge remains stable, whatever the reactions conditions and the nature of the molecule. The stable configurations (3A, 3B, 3C for 2MT and 4A, 4B, 4C for 23DMB1N) correspond to similar reconstruction of the S-edge as shown in Figs. 7 and 8. In the case of 23DMB1N, the ΔE_{ads} value does not compensate for the loss of energy due to the S-edge reconstruction which explains why the 23DMB1N molecule is strongly destabilized.

Comparing the two CoMoS edges, we conclude that the S-edge exhibit a much higher selectivity index than the M-edge. This behavior should help for the rational choice of the morphologies with predominant S-edges for selective adsorption.

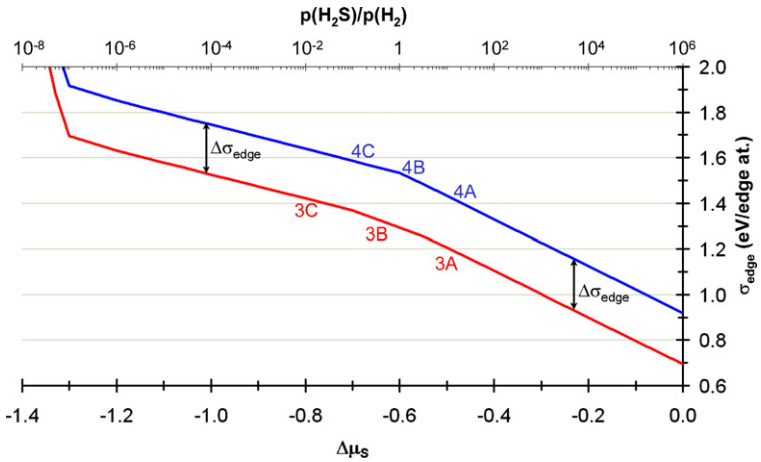

Fig. 15. Edge energy diagram of molecules adsorbed on CoMoS S-edge with full Co decoration as a function of $\Delta\mu_S$. The p_{H_2S}/p_{H_2} axis is determined for $T = 523$ K. (Blue line: 23DMB1N, red line: 2MT). (For interpretation of the references to color in this figure legend, the reader is referred to the web version of this article.)

4.2. NiMoS

On the NiMoS S-edge, Fig. 16 shows that the adsorption selectivity of both molecules varies with the reaction conditions and the promoter content. While the selectivity index of the totally promoted edge (full lines) is close to null ($\Delta\sigma_{S\text{-edge}} = -0.03$ eV/edge atom), the presence of mixed –Ni–Mo–Ni–Mo– sites induces a decrease of selectivity ($\Delta\sigma_{M\text{-edge}} = -0.16$ eV/edge atom for the dashed lines). This value is close to the Co-promoted M-edge. In particular, it is important to underline that the 5C configuration of 2MT stabilized in HDS conditions reveal that it is possible to exchange the remaining sulfur atom by the thiophene molecule. This configuration is not possible with 23DMB1N for which ΔE_{ads} does not counterbalance the energy cost for the sulfur removal. This highlights that the decrease of the Ni content at the M-edge may improve the adsorption selectivity of 2MT.

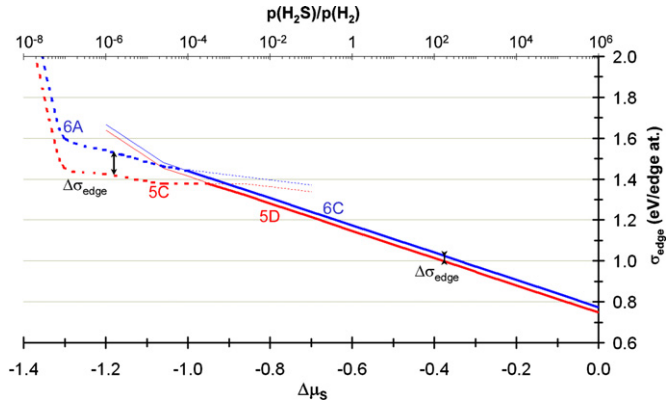

Fig. 16. Edge energy diagram of molecules adsorbed on NiMoS M-edge as a function of $\Delta\mu_S$. The p_{H_2S}/p_{H_2} axis is determined for $T = 523$ K. (Blue line: 23DMB1N, red line: 2MT, full line: fully promoted edge, dashed line: partially promoted edge). (For interpretation of the references to color in this figure legend, the reader is referred to the web version of this article.)

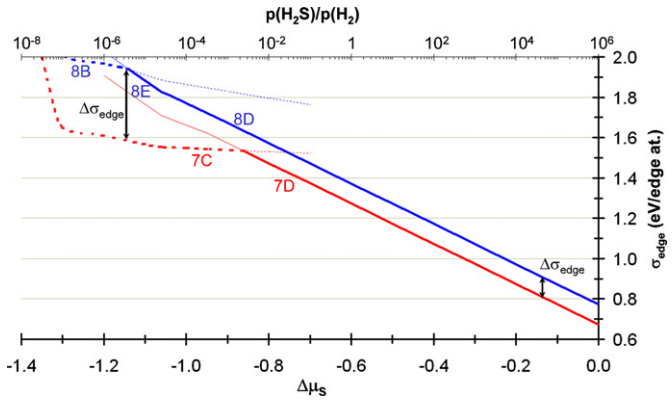

Fig. 17. Edge energy diagram of the molecules adsorbed on NiMoS S-edge as a function of $\Delta\mu_S$. The p_{H_2S}/p_{H_2} axis is determined for $T = 523$ K. (Blue line: 23DMB1N, red line: 2MT, full line: fully promoted edge, dashed line: partially promoted edge). (For interpretation of the references to color in this figure legend, the reader is referred to the web version of this article.)

For the S-edge (Fig. 17), we observe similar tendencies. The totally promoted edge exhibits a weak selectivity index ($\Delta\sigma_{S\text{-edge}} = -0.09$ eV/edge atom), whereas the $\Delta\sigma_{S\text{-edge}}$ is significantly reduced (−0.36 eV/edge atom) for the partially decorated edge (i.e. mixed edge), also found in the more reductive environment.

Hence, the 23DMB1N will be strongly inhibited by 2MT for $\Delta\mu_S < -0.86$ eV (i.e. HDS reaction conditions), due to the presence of mixed –Ni–Mo–Ni–Mo sites stabilizing the 2MT molecule in the configuration 7C (Fig. 12). As for the M-edge, the energy gain by the 2MT adsorption is strong enough to counterbalance, the energy loss resulting from the S-removal.

As a consequence, we find that the adsorption selectivity of both NiMoS edges depends on reaction conditions and also on the promoter content. Due to the presence of the mixed sites, the adsorption selectivity of NiMoS can be increased with respected to the totally promoted system. This result is important for improving the catalytic active phase: it reveals that higher adsorption selectivity might be provided by favoring the partial decoration of Ni at the edges. It is also worth to underline that the S-edge is always more selective than the M-edge, as already found for CoMoS.

4.3. Kinetic interpretation

Volcano shape correlations have been proposed in recent studies investigating numerous model reactions involved in HDS and HDT between the calculated sulfur–metal bond energy E(MS) descriptor, and the HDS turnover frequency (TOF) [3,10–12], or the olefin hydrogenation (HydO) TOF [3]. A different periodic trend in HDS was earlier proposed in the literature [64], using however a different bulk energy descriptor. We recall that the E(MS) energy, as defined and used in [3,10–12] is calculated for the bulk transition metal sulfide phases stable in HDS conditions. The larger the E(MS) value is, the stronger the M–S bond. The Mo–S bond has been calculated to be stronger than the Co–S bond in CoMoS, the latter being stronger than the Ni–S bond in NiMoS.

A first attempt was recently proposed to extend this volcano curve to HDS/HydO selectivity on the basis of fitted volcano curves and experimental catalytic tests [3,9]. Indeed depending on the relative positions and shapes of the two HDS and HYD volcanoes, one can suspect that the selectivity will change as a function of the catalyst. Fig. 18 reports such volcanoes for HydO activity and

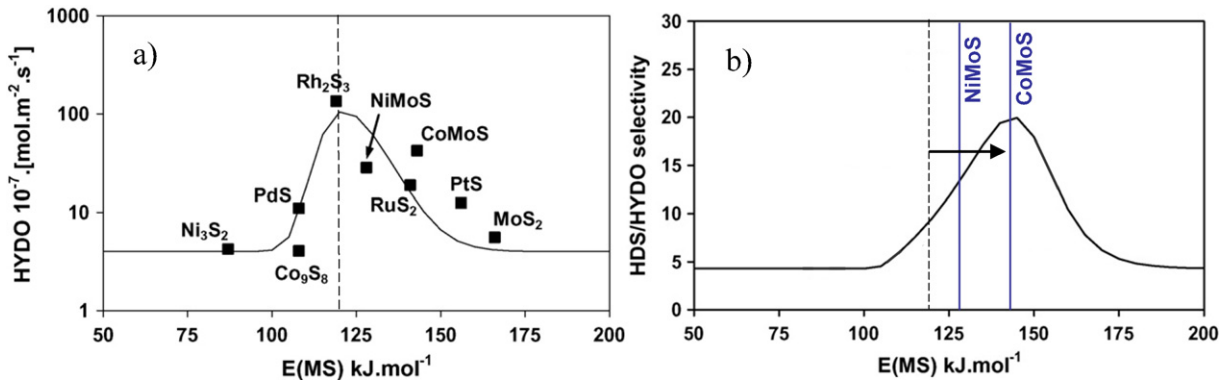

Fig. 18. Volcano-curves kinetic models of (a) HydO activity of 23DMB2N, (b) HDS/HydO selectivity as a function of E(MS). The curves represent the best fitted microkinetic models and full squares represent the experimental data of Ref. [9]. The arrow indicates the shift between the position of the HydO activity maximum (dashed line) and the HDS/HydO selectivity maximum (adapted from [3,9]).

HDS/HYDO selectivity obtained in the recent work by Daudin et al. [9].

The kinetic model developed in [9] is based on a Langmuir–Hinshelwood model with 2MT and 23DMB1N competing for the same catalytic active site. The rate determining step of the HDS and HydO reactions has been found to be the first hydrogen transfer from the M–SH groups to the adsorbed molecules. This model assumes that Brønsted–Evans–Polanyi (BEP) relationships exist between activation energies of the rate determining step and E(MS) as well as linear relationships between adsorption energies and E(MS). This assumption was proposed in absence of any DFT calculated data for the whole range of transition metal sulfides surfaces, which would require a specific investigation beyond the scope of the present work.

The kinetic models reported in Fig. 18 shows that the optimum of the selectivity volcano is shifted to the E(MS) value close to 145 kJ/mol, which is higher than the optima found for HDS or HYDO activities (close to 120–125 kJ/mol, dashed line in Figs. 18). In particular, this model recovers that the CoMoS active phase (E(MS) ∼143 kJ/mol) should be more selective than NiMoS (E(MS) ∼128 kJ/mol), the latter being often described as "more hydrogenating." This general trend is also consistent with the DFT selectivity adsorption index, $\Delta\sigma_{\text{edge}}$, which is found to be more negative on CoMoS than on NiMoS in the case of the fully promoted edges (as presented in the previous section).

Fitting the kinetic parameters with experimental data allowed to sketch linear relationships between activation–adsorption energies and E(MS). The fitted activation enthalpies of the rate determining step were evaluated at $\Delta G^{\neq}(\text{HydO}) = +59$ kJ/mol for HydO of 23DMB1N and $\Delta G^{\neq}(\text{HDS}) = +109$ kJ/mol for HDS of 2MT [9]. The selectivity (ratio of the HDS and HydO TOFs) is expressed as a function of the coverages, θ, of MT, 23DMB1N and –SH species involved in the two HDS and HydO rate determining steps:

$$\frac{r(\text{HDS})}{r(\text{HydO})} = \frac{k_{\text{HDS}}\theta_{\text{MT}}\theta_{\text{SH}}}{k_{\text{HydO}}\theta_{\text{23DMB1N}}\theta_{\text{SH}}} = e^{-\frac{\delta\Delta G^{\neq} + 4\Delta\sigma_{\text{edge}}}{RT}}, \tag{11}$$

where $\delta\Delta G^{\neq} = \Delta G^{\neq}(\text{HDS}) - \Delta G^{\neq}(\text{HydO}) \approx +50$ kJ/mol, according to [9].

Hence, in order to obtain selectivity significantly greater than 1, the $\delta\Delta G^{\neq}$ term must be counterbalanced by the $\Delta\sigma_{\text{edge}}$ term which must become inferior to the critical value of ~ -12.5 kJ/mol (i.e. −0.13 eV/edge atom).

According to the DFT results, this criterion is generally verified for the CoMoS edges: $\Delta\sigma_{S\text{-edge}} \sim -0.22$ eV/edge atom and $\Delta\sigma_{M\text{-edge}} \sim -0.15$ eV/edge atom in the HDS conditions.

Fig. 19 recalls the linear relationships for adsorption energies of reactants and species involved in the HDS and HydO mechanisms, according to Ref. [9]. These relationships are consistent with the DFT calculations (Figs. 14 and 15), showing that the 23DMB1N is less strongly adsorbed on the edges. According to the linear relationships, the adsorption energies for 2MT and the 23DMB1N are respectively −116 kJ/mol (i.e. −1.21 eV) and −66 kJ/mol (i.e. −0.69 eV) on CoMoS. These values are in agreement with DFT adsorption energies computed on CoMoS. Depending on the promoter contents and sulfur coverages, they comprise between −0.97 and −1.39 eV for 2MT and between −0.43 and −0.73 eV for 23DMB1N (Tables 1–4). Hence, both the kinetic model and the DFT calculations show that the adsorption selectivity index of CoMoS counterbalances the critical value of $\delta\Delta G^{\neq}$.

In contrast, the NiMoS edges do not always verify the criterion. Even if the general effect of Ni is to lower the adsorption energies of both molecules (as obtained by kinetic modeling and by DFT calculations), a direct comparison in adsorption energies between DFT and the kinetic model is more complex to establish for the NiMoS M- and S-edges. Actually, two interconnected

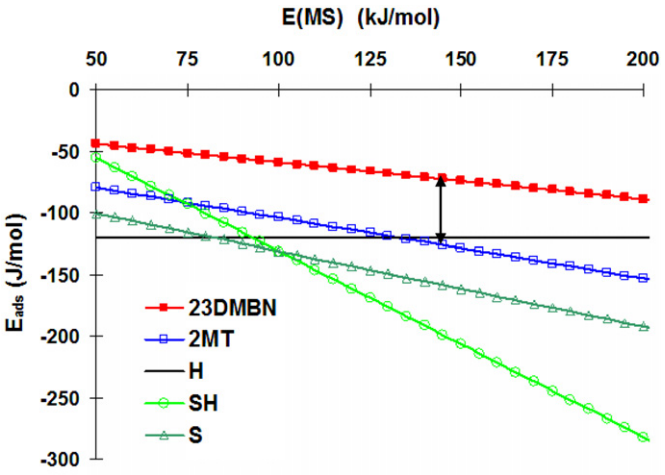

Fig. 19. Linear relationships between adsorption energies of the different species involved in the elementary steps of HDS and HydO and the E(MS) descriptor. The arrow represents the adsorption energy difference between 2MT and 23DMBN (adapted from [9]).

effects must be considered: the Ni content at the edges and the partial pressure of H_2S. On the one hand, reducing the Ni content at the edge (as found in more reductive environment), increases the sulfur–metal bond energy [26], and shifts E(MS) closer to the CoMoS value. According to the DFT calculations (Figs. 16 and 17), while the $\Delta\sigma_{\text{edge}}$ values of the NiMoS fully promoted edges are not less than −0.09 eV/edge atom, the partial decoration of the NiMoS edge improves the adsorption selectivity index (−0.16 and −0.36 eV/edge atom, comparable to CoMoS) counterbalancing the critical value of $\delta\Delta G^{\neq}$. In that case, NiMoS becomes more selective as illustrated by the experimental observations of Ref. [9]. This result suggests also that the NiMoS catalyst is more sensitive to the promoter edge content, with respect to HDS/HydO selectivity and may be improved as a function of this key parameter. The experimental data obtained in Ref. [9] seems to reveal that it is possible to prepare NiMoS catalysts, probably with a higher number of mixed Ni–Mo sites, leading to an improved selectivity.

Finally, the role of the partial pressure of H_2S cannot be excluded. It has been shown that the effect of H_2S may be at the origin of the decrease in HydO activity of NiMoS with respect to CoMoS [4]. Assuming that the promoter content keeps constant, the increase of the partial pressure of H_2S (i.e. chemical potential of S) would imply an increase of S-species at the edge becoming strong adsorption inhibitors of 23DMB1N at the NiMoS edges (Fig. 19), where the calculated adsorption energies of 23DMB1N are found the least exothermic.

5. Conclusions

Using periodic DFT calculations, we have investigated the selective adsorption of two relevant model molecules (2MT and 23DMB1N) in HDS and HydO reactions on Co(Ni)MoS active phase, as a function of the sulfo-reductive environment. The main insights obtained in the present work are the following.

- The selective adsorption of reactants is suggested as a key parameter controlling the HDS/HydO selectivity in Co(Ni)MoS phase. In all cases, the 23DMB1N molecule is inhibited by the 2MT molecule.
- The DFT descriptor, called $\Delta\sigma_{\text{edge}}$, is proposed to quantify the adsorption selectivity of thiophene derivatives and olefins.
- The adsorption configurations for the two molecules are also explained by the quantification of ELF basins population.

- Whatever the reaction conditions, the S-edge of Co(Ni)MoS has been found to be more selective than the M-edge. Consequently, nano-crystallites with morphologies maximizing the S-edge/M-edge ratio should exhibit improved HDS/HydO selectivity.
- Whereas the Co content on the edges has been found to hardly influence the adsorption selectivity, the Ni edge content is a key parameter for NiMoS. A partial decoration of the edges (with mixed Ni–Mo sites) should increase the adsorption selectivity of thiophene derivatives on the NiMoS active phase.
- The DFT calculated adsorption energies of 2MT (model molecule for HDS) and 23DMB1N (model molecule for HydO) on CoMoS and NiMoS are consistent with the fitted values used in the kinetic model recently proposed in the literature [9].
- In coherence with volcano-curve relationships, we have found that favoring such mixed Ni–Mo sites may improve HDS/HydO selectivity, by increasing the sulfur–metal bond energy closer to the optimum of the volcano curve.

References

[1] R. Prins, in: G. Ertl, H. Knözinger, J. Weitkamp (Eds.), Handbook of Heterogeneous Catalysis, vol. 4, Wiley–VHC Verlagsgesellschaft, Weinheim, 1997, p. 1908.
[2] H. Topsøe, B.S. Clausen, F.E. Massoth, in: J.R. Anderson, M. Boudart (Eds.), Hydrotreating Catalysis—Science and Technology, Springer-Verlag, Berlin/Heidelberg, 1996, vol. 11.
[3] A. Daudin, S. Brunet, G. Perot, P. Raybaud, C. Bouchy, J. Catal. 248 (2007) 111.
[4] A.F. Lamic, A. Daudin, S. Brunet, C. Legens, C. Bouchy, E. Devers, Appl. Cat. A 344 (2008) 198.
[5] D. Mey, S. Brunet, C. Canaff, F. Maugé, C. Bouchy, F. Diehl, J. Catal. 227 (2004) 436.
[6] S. Brunet, D. Mey, G. Perot, C. Bouchy, F. Diehl, Appl. Catal. A 278 (2005) 143.
[7] J.T. Miller, W.J. Reagan, J.A. Kaduk, C.L. Marshall, A.J. Kropf, J. Catal. 193 (2000) 123–131.
[8] J.-S. Choi, F. Mauge, C. Pichon, J. Olivier-Fourcade, J.-C. Jumas, C. Petit-Clair, D. Uzio, Appl. Catal. A 267 (2004) 203.
[9] A. Daudin, A.F. Lamic, G. Perot, S. Brunet, P. Raybaud, C. Bouchy, Catal. Today 130 (2008) 221.
[10] H. Toulhoat, P. Raybaud, S. Kasztelan, G. Kresse, J. Hafner, Catal. Today 50 (1999) 629.
[11] R.R. Chianelli, G. Berhault, P. Raybaud, S. Kasztelan, J. Hafner, H. Toulhoat, Appl. Catal. A 227 (2002) 83.
[12] H. Toulhoat, P. Raybaud, J. Catal. 216 (2003) 63.
[13] J.V. Lauritsen, M.V. Bollinger, E. Lægsgaard, K.W. Jacobsen, J.K. Nørskov, B.S. Clausen, H. Topsøe, F. Besenbacher, J. Catal. 221 (2004) 510.
[14] J.V. Lauritsen, J. Kibsgaard, G.H. Olesen, P.G. Moses, B. Hinnemann, S. Helveg, J.K. Nørskov, B.S. Clausen, H. Topsøe, E. Laegsgaard, F. Besenbacher, J. Catal. 249 (2007) 220.
[15] S.M.A.M. Bouwens, J.A.R. van Veen, D.C. Koningsberger, V.H.J. de Beer, R. Prins, J. Phys. Chem. 95 (1991) 123.
[16] S. Kasztelan, H. Toulhoat, J. Grimblot, J.P. Bonnelle, Appl. Catal. 13 (1984) 127.
[17] H. Schweiger, P. Raybaud, H. Toulhoat, J. Catal. 212 (2002) 33.
[18] E. Krebs, B. Silvi, P. Raybaud, Catal. Today 130 (2008) 160.
[19] H. Schweiger, P. Raybaud, G. Kresse, H. Toulhoat, J. Catal. 207 (2002) 76.
[20] P. Raybaud, Appl. Catal. A 322 (2007) 76.
[21] L.S. Byskov, J.K. Nørskov, B.S. Clausen, H. Topsøe, J. Catal. 187 (1999) 109.
[22] A. Travert, H. Nakamura, R.A. van Santen, S. Cristol, J.F. Paul, E. Payen, J. Am. Chem. Soc. 124 (2002) 7084.
[23] M. Sun, A.E. Nelson, J. Adjaye, J. Catal. 226 (2004) 32.
[24] P. Raybaud, J. Hafner, G. Kresse, S. Kasztelan, H. Toulhoat, J. Catal. 189 (2000) 129.
[25] L.S. Byskov, J.K. Norskov, B.S. Clausen, H. Topsoe, Catal. Lett. 64 (2000) 95.
[26] P. Raybaud, J. Hafner, G. Kresse, S. Kasztelan, H. Toulhoat, J. Catal. 190 (2000) 128.
[27] S. Cristol, J.F. Paul, E. Payen, D. Bougeard, F. Hutschka, S. Clemendot, J. Catal. 224 (2004) 138.
[28] S. Cristol, J.F. Paul, C. Schovsbo, E. Veilly, E. Payen, J. Catal. 239 (2006) 145.
[29] J.-F. Paul, S. Cristol, Catal. Today 130 (2008) 139.
[30] P. Raybaud, J. Hafner, G. Kresse, H. Toulhoat, Phys. Rev. Lett. 80 (1998) 1481.
[31] M. Sun, A.E. Nelson, J. Adjaye, Catal. Lett. 109 (2006) 133.
[32] H. Orita, K. Uchida, N. Itoh, Appl. Catal. A 258 (2004) 115.
[33] T. Weber, J.A.R. Van Veen, Catal. Today 130 (2008) 170.
[34] M.Y. Sun, A.E. Nelson, J. Adjaye, J. Catal. 231 (2005) 223.
[35] M.Y. Sun, A.E. Nelson, J. Adjaye, Catal. Today 109 (2005) 49.
[36] T. Todorova, R. Prins, T. Weber, J. Catal. 236 (2005) 190.
[37] P.G. Moses, B. Hinnemann, H. Topsoe, J. Norskov, J. Catal. 248 (2007) 188–203.
[38] J.P. Perdew, Y. Wang, Phys. Rev. B 45 (1992) 13244.
[39] J.P. Perdew, J.A. Chevary, S.H. Vosko, K.A. Jackson, M.R. Pederson, D.J. Singh, C. Fiolhais, Phys. Rev. B 46 (1992) 6671.
[40] G. Kresse, J. Furthmüller, Comput. Mater. Sci. 6 (1996) 15.
[41] G. Kresse, J. Furthmüller, Phys. Rev. B 54 (1996) 11169.
[42] P. Hohenberg, W. Kohn, Phys. Rev. B 136 (1964) 864.
[43] W. Kohn, L.J. Sham, Phys. Rev. A 140 (1965) 1133.
[44] G. Kresse, D. Joubert, Phys. Rev. B 59 (1999) 1758.
[45] C. Arrouvel, M. Breysse, H. Toulhoat, P. Raybaud, J. Catal. 232 (2005) 161.
[46] F. Mittendorfer, C. Thomazeau, P. Raybaud, H. Toulhoat, J. Phys. Chem. B 107 (2003) 12287.
[47] A.D. Becke, K.E. Edgecombe, J. Chem. Phys. 92 (1990) 5397.
[48] B. Silvi, J. Phys. Chem. A 107 (2003) 3081.
[49] B. Silvi, A. Savin, Nature 371 (1994) 683.
[50] E. Matito, B. Silvi, M. Duran, M. Sol, J. Chem. Phys. 125 (2006) 024301.
[51] G.N. Lewis, J. Am. Chem. Soc. 38 (1916) 762.
[52] G.N. Lewis (Ed.), Valence and the Structure of Atoms and Molecules, Dover, New York, 1966.
[53] A.D. Becke, J. Chem. Phys. 98 (1993) 5648.
[54] C. Lee, Y. Yang, R.G. Paar, Phys. Rev. B 37 (1988) 785.
[55] K.D. Dobbs, W.J. Hehre, J. Comput. Chem. 8 (1987) 880.
[56] M.J. Frisch et al., Gaussian 03, revision C. 02, Gaussian Inc., Pittsburgh, PA, 2003.
[57] S. Noury, X. Krokidis, F. Fuster, B. Silvi, Topmod package, 1997.
[58] S. Noury, X. Krokidis, F. Fuster, B. Silvi, Comput. Chem. 23 (1999) 597.
[59] R.H. Abraham, C.D. Shaw (Eds.), Dynamics: The Geometry of Behavior, Addison–Wesley, 1992.
[60] R.H. Abraham, J.E. Marsden (Eds.), Foundations of Mechanics, Addison–Wesley, 1994.
[61] Template Graphics Software TGS, Inc., San Diego, USA, Amira 3.0, 2002.
[62] M.Y. Sun, A.E. Nelson, J. Adjaye, Catal. Today 105 (2005) 36.
[63] M.Y. Sun, A.E. Nelson, J. Adjaye, J. Catal. 233 (2005) 411.
[64] J.K. Nørskov, B.S. Clausen, H. Topsøe, Catal. Lett. 13 (1992) 1.